[CANCER RESEARCH 63, 5950–5956, September 15, 2003]

Endothelial Apoptosis Initiates Acute Blood–Brain Barrier Disruption after Ionizing Radiation[1]

Yu-Qing Li, Paul Chen, Adriana Haimovitz-Friedman, Raymond M. Reilly, and C. Shun Wong[2]

Department of Radiation Oncology, Sunnybrook and Women's College Health Sciences Center, University of Toronto, Toronto, Ontario, M4N 3M5 Canada [Y-Q. L., C. S. W.]; Division of Nuclear Medicine, Toronto General Hospital, University Health Network, University of Toronto, Toronto, Ontario, M5G 2C4 Canada [P. C., R. M. R.]; and Memorial Sloan-Kettering Cancer Center, New York, New York 10021 [A. H-F.]

ABSTRACT

Acute disruption of blood–brain barrier (BBB) is well recognized after radiation therapy to the central nervous system (CNS). We assessed the genetic regulation of acute BBB disruption and its relationship to vascular endothelial cell death in the CNS after irradiation. Adult rats were given graded single doses of X-ray to the cervical spinal cord. At different time intervals after irradiation, the irradiated spinal cord was processed for histological and immunohistochemical analysis. Disruption of blood–spinal cord barrier was assessed using albumin immunohistochemistry, i.v. injection of Evans blue dye, and ^{99m}Tc-diethylenetriamine pentaacetic acid. In the rat spinal cord, there was a dose-dependent apoptotic response during the first 24 h after irradiation, and apoptotic cells consisted of both endothelial and glial cells, as described previously (1, 2). A dose-dependent reduction in endothelial cell density was observed at 24 h after irradiation. This was associated with a similar dose-dependent disruption in blood–spinal cord barrier as demonstrated by albumin immunohistochemistry. Radiation-induced apoptosis in endothelial cells has been shown to be dependent on the acid sphingomyelinase (ASMase) pathway. After a single 50-Gy dose to the cervical spinal cord of ASMase +/+ mice, there was a 47.7% reduction in endothelial cell density at 24 h compared with nonirradiated controls. No decrease in endothelial cell density was observed in irradiated ASMase −/− mice. In the irradiated spinal cord of ASMase +/+ mice, there was evidence of albumin immunoreactivity and Evans blue dye staining around microvessels, and ^{99m}Tc-diethylenetriamine pentaacetic acid uptake increased at 24 h. Nonirradiated controls and the irradiated spinal cord of ASMase −/− mice demonstrated no evidence of leakage. We conclude that apoptosis of endothelial cells initiates acute BBB disruption in the CNS after irradiation and that acute BBB disruption after irradiation is mediated by the ASMase pathway.

INTRODUCTION

The CNS[3] is one of the major dose-limiting organs in clinical radiotherapy. Undoubtedly, the late irreversible CNS injury after XRT is most important clinically. However, acute clinical effects are also well recognized. These consist of nonspecific constitutional symptoms and an increase in neurological symptoms, often within a few hours, particularly after large doses per fraction. Although previous studies reported little evidence of injury at these early times at the histological level (3), recent studies have described alterations in gene and protein expression (4–6). In the CNS, oligodendrocytes (1, 7), subependymal cells (8, 9), and endothelial cells (9) have been shown to undergo apoptosis within the first 24 h after XRT. How these events relate to the acute clinical symptoms remains largely unknown.

Although not as well defined in the CNS, acute vascular changes such as endothelial cell swelling, thickening of the basal lamina, vasculation of cytoplasm, vascular permeability, and edema have been observed within 24 h after XRT (10). In the CNS, the endothelial cell, strengthened by tight junctions and having low rates of fluid-phase endocytosis, defines the BBB (11). Disruption of the BBB is consistently observed at early times after XRT. Using Evans blue dye as a vascular tracer, Siegal *et al.* (4) demonstrated an increase in vascular permeability at 18 h after a single dose of 15 Gy. This was associated with a decrease in levels of endothelin, a potent vasoconstrictor.

Microvascular endothelial apoptosis has been demonstrated to play a critical role in XRT pneumonitis (12) and, more recently, in XRT-induced crypt damage and death from the gastrointestinal syndrome (13). Endothelial apoptosis has been observed within 24 h after XRT in the CNS (2). In rat brain, a single dose of 25–100 Gy produced a 15% loss of endothelial cells within 24 h (14). This was consistent with endothelial cell apoptosis observed during the first 24 h after XRT.

In vitro and *in vivo*, XRT-induced endothelial cell apoptosis is mediated by the lipid second messenger ceramide via activation of ASMase (15, 16). This pathway is initiated by the hydrolysis of sphingomyelin via the action of sphingomyelinases to generate ceramide. Ceramide then serves as a second messenger in this system, leading to apoptosis (17). Sphingomyelin degradation has been ascribed to at least two distinct sphingomyelinases: ASMase, and NSMase. Both ASMase and NSMase have been implicated in radiation-induced apoptosis (18–20). Recent investigations linked the activation of ASMase to the stress-activated protein kinase/c-jun kinase cascade and apoptotic responses, and NSMase to the extracellular signal-regulated kinase cascade and pro-inflammatory responses (21, 22). XRT-induced apoptosis was found to be defective in endothelial cells of ASMase −/− mice, suggesting that the activation of ASMase plays a critical role in XRT-induced apoptosis (2, 13, 23). However, whether apoptotic damage to the microvasculature plays a role in the pathogenesis of acute XRT damage to the CNS remains unclear.

We postulated that the acute loss of endothelial cells is associated with endothelial cell apoptosis. We further postulated that endothelial cell apoptosis leads to acute disruption of the BBB. In this study, we demonstrate a reduction in endothelial cell density and disruption of the BSCB in wild-type but not ASMase knockout animals. These results are thus consistent with the hypothesis that there is a causal relationship between acute endothelial cell apoptosis and BBB disruption and that the ASMase pathway plays a critical role in acute BBB disruption in the CNS after XRT.

MATERIALS AND METHODS

Animals. Female Fisher 344 rats, p53 (C57BL6/J strain; The Jackson Laboratory, Bar Harbor, ME) and ASMase mice (obtained from Memorial Sloan-Kettering Cancer Center, New York, NY, and rederived at the Ontario Cancer Institute), 8–9 weeks of age, were used in this study. Litters from ASMase heterozygous breeding pairs of C57B1/6 × 129SVEV genetic background were genotyped at 4 weeks of age (24). The animals were fed a standard rodent diet and given water *ad libitum* in the animal colony of the

Received 4/11/03; revised 6/9/03; accepted 6/27/03.

The costs of publication of this article were defrayed in part by the payment of page charges. This article must therefore be hereby marked *advertisement* in accordance with 18 U.S.C. Section 1734 solely to indicate this fact.

[1] Supported by the National Cancer Institute of Canada (C. S. W.) with funds from the Canadian Cancer Society.

[2] To whom requests for reprints should be addressed, at Department of Radiation Oncology, Sunnybrook and Women's College Health Sciences Center, 2075 Bayview Avenue, Toronto, Ontario, M4N 3M5 Canada. Phone: (416) 480-4619; Fax: (416) 480-5737; E-mail: shun.wong@tsrcc.on.ca.

[3] The abbreviations used are: CNS, central nervous system; XRT, radiation treatment; BBB, blood–brain barrier; ASMase, acid sphingomyelinase; NSMase, neutral sphingomyelinase; BSCB, blood-spinal cord barrier; TUNEL, terminal dUTP nicked end labeling; DAPI, 4,6-diamidino-2-phenylindole; DTPA, diethylenetriamine pentaacetic acid.

Ontario Cancer Institute, a laboratory animal colony accredited by the Canadian Council of Animal Care. All experimental protocols involving animals were approved by the Animal Care Committee of the Ontario Cancer Institute.

Irradiation. Animals were immobilized during XRT in a polystyrene foam jig and with inhalation anesthesia with halothane. The cervical spinal cord (C2–T2) was irradiated by two Picker Gemini 100-kV X-ray units used in a parallel, opposed configuration. Check films for accuracy of field placement and *in vivo* thermoluminescence dosimetry were performed before the experiments. Details of XRT methods were as described previously (25).

Rats were irradiated with a single dose of 0, 2, 8, 19.5, 22, 30, or 50 Gy. Single doses of 19.5 and 22 Gy represented the ED_{50} and ED_{100}, respectively, for forelimb paralysis within 180 days secondary to white matter necrosis in the rat spinal cord model (25). A much higher radiation dose was required to induce paralysis in mice, and studies in mice yielded ED_{50} doses of 46–55 Gy for myelopathy (26–28). Transgenic mice were thus irradiated with a single dose of 50 Gy. Control rats and mice were not irradiated. A minimum of three animals were used at each experimental time point, unless otherwise indicated.

Histopathology. Animals were anesthetized with i.p. ketamine (Bimeda-MTC Animal Health Inc., Cambridge, Ontario, Canada) at 0.075 ml/100 g of body weight and Rompun (Bayer Inc., Toronto, Ontario, Canada) at 0.03 ml/100 g dissolved in sterilized physiological saline. After a 1-min transcardiac perfusion with 0.9% saline to clear blood from the circulatory system, animals were perfused with a 10-min transcardiac infusion of 10% buffered-neutral formalin. The spinal cord was dissected out, and sections were obtained by cutting the spinal cord transversely at mid-plane between C2 and T2. Specimens were processed by a standard paraffin embedding method between 48 and 72 h after XRT and cut at 4-μm thickness for routine H&E and immunohistochemical studies.

Assessment of Apoptosis. For assessment of apoptosis, animals were sacrificed at 8 or 10 h after XRT. Identification of apoptotic cells was based on standard morphological criteria under light microscopy at $\times$1000 magnification on H&E-stained sections as described previously (1, 7). Briefly, cells that showed cell shrinkage and nuclear condensation or fragmentation were considered apoptotic cells, and apoptotic cells on vascular microvessel walls or inside microvessels were considered vascular endothelial cells undergoing XRT-induced apoptosis. Selected slides were processed for TUNEL with use of the *In situ* Cell Death Detection Kit (Boehringer Mannheim Canada, Laval, Québec, Canada). As described previously (1, 29), deparaffinized sections were incubated with proteinase K and were sequentially incubated with TUNEL reaction mixture (Boehringer Mannheim Canada) after washing in PBS. The tagged ends were labeled with an antibody conjugated to FITC (Dako Diagnostics Canada Inc., Mississauga, Ontario, Canada). The sections were then stained with laminin conjugated with Cy3 (Sigma, St. Louis, MO) and counterstained with DAPI (Sigma) to further confirm apoptotic endothelial cells. The microscopic filter used for TUNEL staining was temporarily changed when a TUNEL-positive cell was observed during counting to determine whether there was nuclear condensation or fragmentation in DAPI staining to avoid TUNEL false positive staining, *i.e.,* artifact.

Immunohistochemistry. Sections were deparaffinized in toluene and rehydrated through a graded alcohol series. Endogenous peroxidase activity was blocked in 3% H_2O_2. After pretreatment with pepsin for albumin (Biogenesis Inc., Poole, England), laminin (Sigma), and factor VIII-related antigen (Dako Diagnostics Canada) immunohistochemistry, the sections were incubated with the respective primary antibodies (1:6400 dilution for albumin, 1:200 dilution for laminin, and 1:2000 dilution for factor VIII-related antigen). This was followed by incubations with biotinylated linking antibody and horseradish peroxidase (Dako Diagnostics Canada) with brief rinses in PBS between incubations. The reaction was visualized using 3-amino-9-ethylcarbazole, or NovaRED (Vector Laboratories, Burlingame, CA) and counterstained with Mayer's hematoxylin. Reagent controls (omitting the primary antibody or substituting nonimmune serum for the primary antibody in the staining protocol) on tissue sections revealed no staining, thus confirming the specificity of the primary antibodies used.

Assessment of BSCB Permeability. BSCB permeability was assessed by use of immunohistochemistry for albumin in the CNS parenchyma as a surrogate for disruption of the BSCB (30), and BSCB breakdown was assessed semiquantitatively by use of a MicroComputer Image Device (Imaging Research, Inc., St. Catherine, Ontario, Canada; Ref. 31).

Evans blue dye was applied as a second method to confirm BSCB disruption in the irradiated spinal cord after XRT. Evans blue dye is an azo dye that binds with high affinity to albumin and has intense red fluorescence under rhodamine optics. Evaluation of BSCB breakdown by use of Evans blue dye was based on the method described previously by Fullerton *et al.* (32). Briefly, 200 μl of 4% (w/v) Evans blue (Sigma) in 0.9% saline were injected i.v., and the animals were anesthetized and perfused with 20 ml of PBS and then 20 ml of 4% paraformaldehyde in PBS at 24 h after XRT, or 1 h after Evans blue injection. Tissues were immersed in 30% sucrose in PBS for at least 48 h and embedded in Frozen Tissue Embedding Media (Fisher Scientific, Fair Lawn, NJ). A series of cryostat sections of 10-μm thickness were obtained by cutting the spinal cord transversely at mid-plane between C2 and T2, and BSCB leakage was evaluated at $\times$1000 magnification under fluorescent microscopy (Leica LUX S; Leica Microsystems, Wetzlar, Germany).

The BBB/BSCB permeability tracer ^{99m}Tc-DTPA was used to assess BSCB breakdown quantitatively. ^{99m}Tc-DTPA was prepared by the addition of $Na^{99m}TcO_4$ (Technelite generator; DuPont Pharma, Billerica, MA) and saline to the DTPA-Plus kit (Draximage, Montreal, Québec, Canada). The specificity of ^{99m}Tc-DTPA at injection was 50–75 MBq/mg, and radiochemical purity was >95% as confirmed by thin-layer chromatography.

Mice that were +/+, +/−, or −/− for ASMase received i.v. injections containing 2 MBq of ^{99m}Tc-DTPA at 23 h after the 50-Gy dose. At 24 h after XRT, *i.e.,* 1 h after ^{99m}Tc-DTPA injection, they were sacrificed, blood samples were obtained from the heart, and the segment of the spinal cord (C2–T2) was dissected. Blood and the spinal cord samples were weighed and counted for ^{99m}Tc immediately along with a standard in a gamma counter. Results were expressed as the percentage of the injected dose per gram of tissue and spinal cord-to-blood ratios.

Morphometry. Microvessels that had been cut in transverse sections were analyzed morphometrically. Microvessels only were chosen for analysis because they represent 95% of the blood–tissue interface (33); they were defined as vessels composed of one endothelial cell and basement membrane that was positive for laminin. Microvessels were considered to have been cut transversely if the cell membranes were in sharp focus around the entire circumference and if the ratio of the largest diameter to the smallest diameter was <1.5 (33, 34). Two parameters were used to define endothelial and microvessel density changes in the spinal cord after XRT: (*a*) endothelial cell density, defined as that the total number of endothelial cells that contained a nucleus divided by the transverse cross-sectional area of the spinal cord; and (*b*) microvessel density, defined as that the total number of microvessels that had been transversely sectioned and contained either endothelial cell nucleus or no nucleus, divided by the transverse cross-sectional area of the spinal cord.

Statistical Analysis. All data represent the mean ± SE. Statistical significance was determined by Student's *t* test, except that the Mann–Whitney test was used to determine whether there was a change in endothelial cell density at various time intervals after XRT compared with nonirradiated controls. Data were considered statistically significant at $P < 0.05$. All statistical tests were two-sided. A correlation analysis was used to assess whether there was a dose–response relationship for endothelial cell loss after XRT.

RESULTS

Endothelial Cells Undergo XRT-induced Apoptosis in the Rat and Mouse Spinal Cord. A dose-dependent increase in apoptotic cells was observed in the rat spinal cord at 8 h after XRT, as described previously (1). To demonstrate whether microvascular endothelial cell underwent apoptosis after XRT, we immunostained sections of the irradiated rat and mouse spinal cord with laminin or factor VIII-related antigen, or triple-stained them with TUNEL, laminin, and DAPI. In the irradiated rat spinal cord at 8 or 10 h after XRT, apoptotic cells were evident on the microvessel wall (Fig. 1, *A* and *B*). Triple immunostaining (TUNEL, laminin, and DAPI) of the irradiated mouse (ASMase +/+) spinal cord also showed apoptotic cell along the microvessel wall (Fig. 1, *C–E*).

XRT Induces Acute Loss of Endothelial Cells and BSCB Disruption. To assess whether XRT induced-apoptosis was associated with endothelial cell loss and early BSCB disruption, we studied adjacent sections of the rat spinal cord immunohistochemically, using

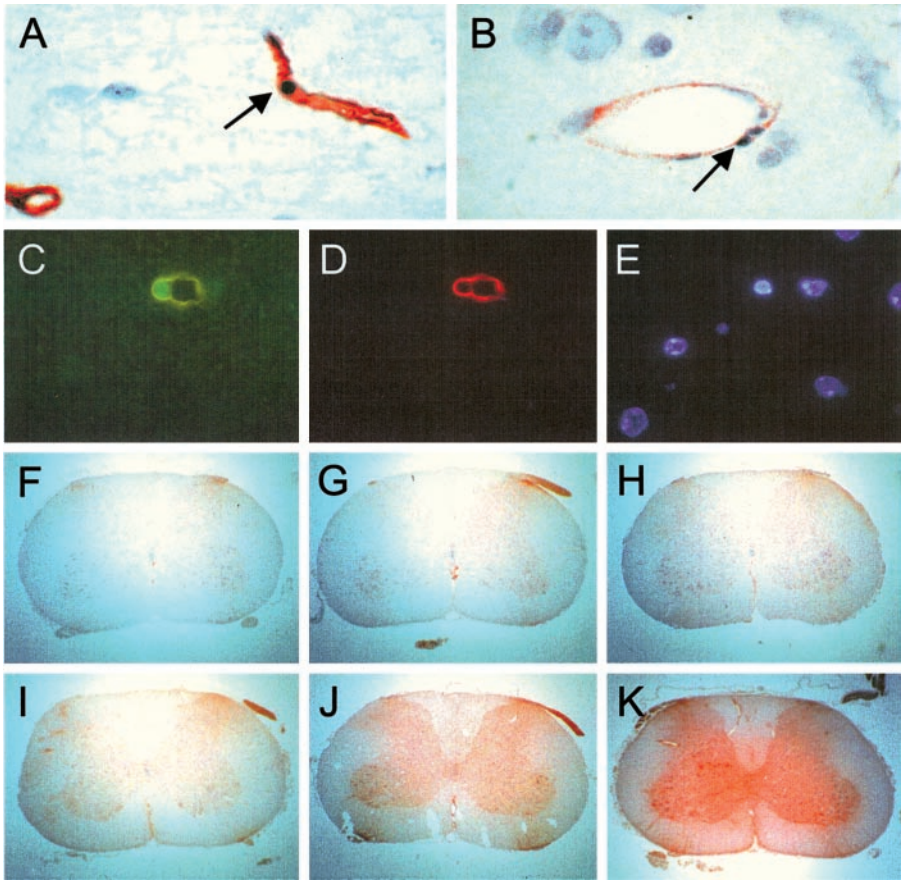

Fig. 1. Vascular endothelial cells in the rat spinal cord undergo XRT-induced apoptosis. *A*, an apoptotic endothelial cell shows nuclear condensation of a microvessel wall (*arrow*, laminin immunohistochemistry) at 10 h after a 22-Gy dose. A laminin-positive microvessel is seen in the background. *B*, apoptotic endothelial cell with two nuclear fragments is observed on a microvessel wall (*arrow*, factor VIII-related antigen immunohistochemistry) at 8 h after a 50-Gy dose. TUNEL assay for detection of apoptosis. *C*, an apoptotic endothelial cell with nuclear condensation is evident as bright staining in the ASMase +/+ mouse spinal cord at 8 h after a 50-Gy dose, as shown in *D* (immunofluorescence staining for laminin) and *E* (counterstained with DAPI). Original magnifications, ×1000. BSCB disruption was assessed with immunohistochemistry using anti-albumin antibody in the rat spinal cord at 24 h in controls (*F*) and after a single dose of 2 (*G*), 8 (*H*), 22 (*I*), 30 (*J*), or 50 Gy (*K*). Original magnifications, ×25.

laminin and albumin, respectively, at various time intervals after graded single doses of X-ray. A significant reduction in endothelial cell density was observed at 12 (25.8% compared with controls; $P = 0.001$), 16 (32.6%; $P = 0.001$), and 24 h (25.7%; $P = 0.002$) after a single dose of 19.5 Gy (Fig. 2, *A* and *B*). For the dose–response experiment, a significant decrease in endothelial cell density was seen only after 50 Gy (39.3% compared with control; $P < 0.01$; Fig. 2*C*). However, the decrease in endothelial cell density correlated with dose consistent with a dose–response relationship ($P < 0.01$). This endothelial cell loss was associated with a similar dose-dependent disruption in BSCB (Fig. 1, *F–K*; Fig. 2*D*).

XRT-induced Endothelial Apoptosis and Cell Loss Are ASMase Dependent. In the three different genotypes of nonirradiated ASMase mouse spinal cord, there was little evidence of apoptosis (0.0~0.7 apoptotic cells/section) and no evidence of endothelial apoptosis. An increase in the number of endothelial apoptosis was observed at 8 h after a single dose of 50 Gy compared with the same genotype controls (Table 1). Triple immunostaining using TUNEL, laminin, and DAPI revealed a 7-fold reduction in the number of apoptotic endothelial cells in ASMase −/− mice compared with wild-type animals (Table 1). The apoptotic response of endothelial cells at 8 h in ASMase +/− animals appeared intermediate compared with that seen in ASMase +/+ and −/− animals.

To assess whether XRT-induced endothelial cell loss at 24 h was causally related to endothelial apoptosis, we measured changes in endothelial cell density in the spinal cord of ASMase +/+ and −/− mice at 24 h after a 50-Gy dose by use of immunohistochemistry for laminin. A significant reduction in endothelial cell density was observed in white (18.7/mm^2 *versus* 9.6/mm^2; $P < 0.01$) and gray matter (48.6/mm^2 *versus* 25.1/mm^2; $P < 0.01$) and the spinal cord section (33.8/mm^2 *versus* 17.6/mm^2; $P = 0.01$) in irradiated ASMase +/+ mice compared with nonirradiated controls (Fig. 3*A*). No decrease in endothelial cell density was observed in ASMase −/− animals after XRT (Fig. 3*B*). The reduction in endothelial density at 24 h after the 50-Gy dose in p53 +/+ mice was similar to that observed in p53 −/− animals (data not shown).

Microvessel density changes in the spinal cord of ASMase +/+ and −/− mice at 24 h after the 50-Gy dose were also assessed by immunohistochemistry for laminin. A significant reduction in microvessel density was observed in white (62.1/mm^2 *versus* 37.7/mm^2; $P = 0.02$) and gray matter (156.2/mm^2 *versus* 88.0/mm^2; $P < 0.01$) and the spinal cord section (109.5/mm^2 *versus* 63.7/mm^2; $P = 0.01$) in irradiated ASMase +/+ mice compared with nonirradiated controls (Fig. 3*C*). ASMase −/− animals showed no decrease in microvessel density after XRT (Fig. 3*D*).

Early BSCB Disruption after XRT Is Mediated by the ASMase Pathway. To investigate whether BSCB disruption is mediated by the ASMase pathway, we assessed BSCB permeability in ASMase +/+, +/−, and −/− mouse spinal cord at 24 h after a 50-Gy dose (Fig. 4). In nonirradiated spinal cord of ASMase +/+ mice (Fig. 4, *A* and *E*), no albumin staining was evident, but diffuse albumin staining was observed after a single dose of 50 Gy (Fig. 4, *B* and *F*). Albumin staining was not evident in nonirradiated (Fig. 4, *C* and *G*) or irradiated ASMase −/− mice (Fig. 4, *D* and *H*).

Similar results were obtained with use of Evans blue dye as a vascular tracer. Nonirradiated ASMase +/+ mouse spinal cord showed no leakage of the dye (Fig. 4, *I* and *M*). Extravasation of Evans blue dye was evident around microvessels in ASMase +/+ spinal cord at 24 h after a 50-Gy dose (Fig. 4, *J* and *N*), but was not observed in nonirradiated (Fig. 4, *K* and *O*) or irradiated ASMase −/− animals (Fig. 4, *L* and *P*).

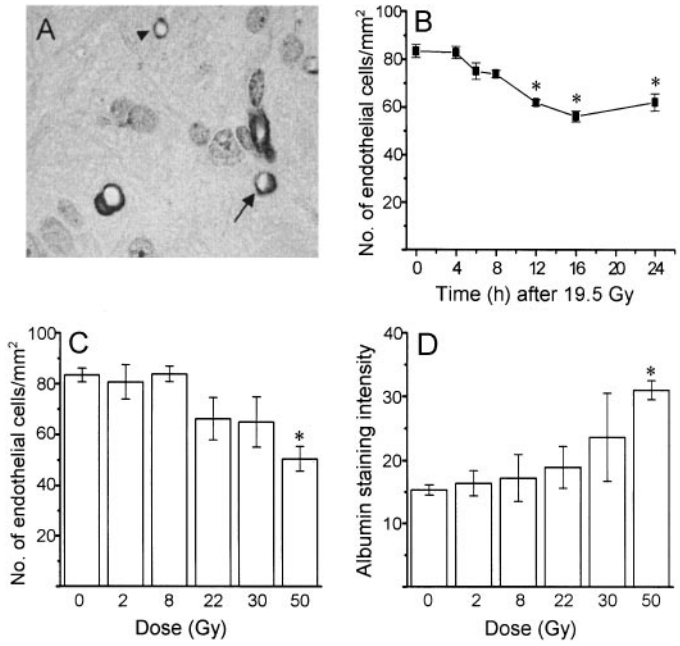

Fig. 2. *A*, laminin immunohistochemistry was used to assess changes of endothelial cell (*arrow*) and microvessel density (*arrowhead*) in the rat spinal cord after XRT. Original magnification, ×1000. *B*, time course of endothelial cell density change in the rat spinal cord after a single dose of 19.5 Gy. Each *data point* represents the mean density of endothelial cells observed in transverse section of the spinal cord from four animals (three sections/animal); *bars*, SE. Nine animals were used at 0 h as controls; ∗, $P \leq 0.002$. *C* and *D*, dose response of endothelial cell density change in transverse section of the rat spinal cord assessed by immunohistochemistry using laminin (*C*) and albumin staining intensity (*D*) on adjacent section was quantified by a MicroComputer Image Device as described in "Materials and Methods" at 24 h after XRT. Each *data point* represents the mean density of endothelial cells or mean of albumin staining intensity in arbitrary unit measured from three animals except nine animals used at 0 Gy as controls (three sections/animal); *bars*, SE. ∗, $P < 0.01$ compared with nonirradiated control obtained by Mann–Whitney test.

Table 1 *XRT-induced endothelial apoptosis in transverse section of ASMase mouse spinal cord at 8 h after 50 Gy using triple immunofluorescence staining of TUNEL, laminin, and DAPI*

	No. of endothelial apoptosis[a]/section
0 Gy, ASMase +/+	0.0 ± 0.0
0 Gy, ASMase +/−	0.0 ± 0.0
0 Gy, ASMase −/−	0.0 ± 0.0
50 Gy, ASMase +/+	2.7 ± 0.3
50 Gy, ASMase +/−	0.6 ± 0.2[b]
50 Gy, ASMase −/−	0.4 ± 0.2[b]

[a] Mean ± SE of six mice, three sections/mouse.
[b] $P \leq 0.004$ compared with 50 Gy, ASMase +/+.

To provide a quantitative assessment of BSCB permeability changes in the three genotypes of ASMase mice, we measured activity for ^{99m}Tc-DTPA in the spinal cord at 24 h after a single dose of 50 Gy (Fig. 5). There was no evidence of ^{99m}Tc-DTPA accumulation in the spinal cord of ASMase −/− mice after XRT. ASMase +/− animals showed an intermediate response compared with that observed in ASMase +/+ and −/− animals. Significant difference in the activity of ^{99m}Tc-DTPA in the spinal cord was observed between irradiated ASMase +/+ animals and nonirradiated controls ($P = 0.025$; Fig. 5*A*). Similar results were seen when we used the spinal cord-to-blood ratio of detected ^{99m}Tc-DTPA ($P < 0.01$; Fig. 5*B*).

In nonirradiated p53 +/+ (Fig. 4*Q*) and −/− mice (Fig. 4*S*), we observed no evidence of albumin immunoreactivity around spinal cord microvessels. Strong albumin staining was seen around microvessels in the spinal cord of both p53 +/+ (Fig. 4*R*) and −/− mice at 24 h after a 50-Gy dose (Fig. 4*T*).

DISCUSSION

In this study, we showed (*a*) that microvascular endothelial cells in the rodent spinal cord undergo XRT-induced apoptosis; (*b*) that a dose-dependent reduction in endothelial cell density observed at 24 h after XRT in the rat spinal cord is associated with a similar dose-dependent disruption in BSCB; (*c*) that a significant reduction in endothelial cell density is observed in the spinal cord of ASMase +/+ mice at 24 h after a 50-Gy dose but not in ASMase −/− mice; (*d*) that in the irradiated spinal cord of ASMase +/+ mice, there is evidence of BSCB disruption at 24 h, whereas the irradiated spinal cord of ASMase −/− mice shows no evidence of BSCB leakage; and (*e*) that the decrease in endothelial density at 24 h after a 50-Gy dose in p53 +/+ mouse spinal cord is similar to that observed in p53 −/− animals, and both p53 +/+ and −/− mouse spinal cord demonstrates BSCB leakage around vessels after XRT.

In nonirradiated mouse or rat spinal cord, spontaneous apoptosis was a rare event. After XRT, apoptotic cells were occasionally observed on the microvessel wall or within microvessels when we used specific immunohistochemical vascular markers and the TUNEL assay, indicating that certain vascular endothelial cells in the CNS were undergoing XRT-induced apoptosis. A significant increase in the number of endothelial apoptosis was observed at 8 h after a single dose of 50 Gy. The apoptotic response of endothelial cells at 8 h in the ASMase +/− animals appeared intermediate compared with that seen in ASMase +/+ and −/− animals. These observations are consistent with previous investigation by Peña *et al.* (2), suggesting that XRT-induced endothelial apoptosis in the CNS is regulated by the ASMase pathway.

In the present study, a decrease in endothelial cell density was noted

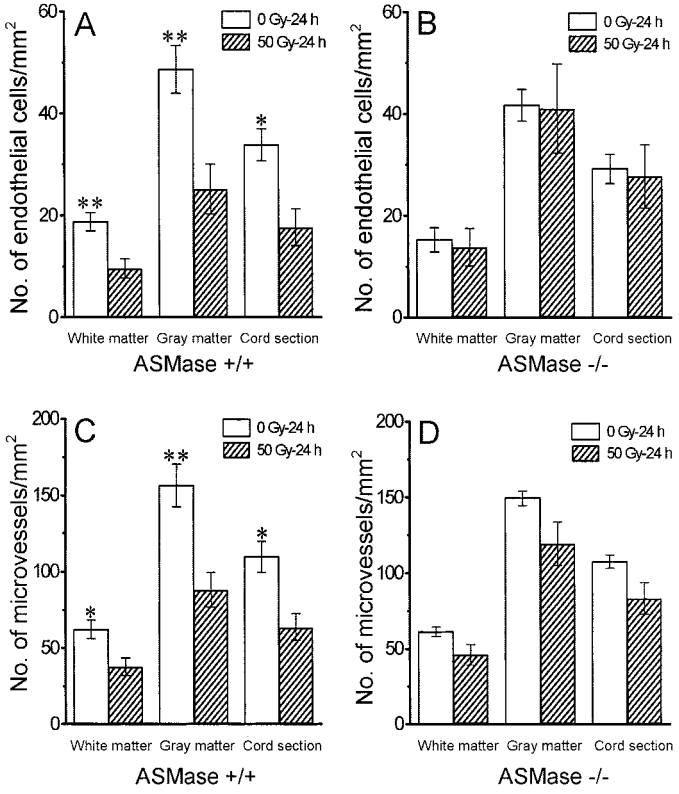

Fig. 3. Endothelial cell (*A* and *B*) and microvessel density (*C* and *D*) changes in the spinal cord of ASMase +/+ (*A* and *C*) and −/− mice (*B* and *D*) at 24 h after a 50-Gy dose assessed by immunohistochemistry for laminin. Each *data point* represents mean density of endothelial cells or microvessels from three animals (three sections/animal); *bars*, SE. ∗, $P < 0.05$; ∗∗, $P < 0.01$.

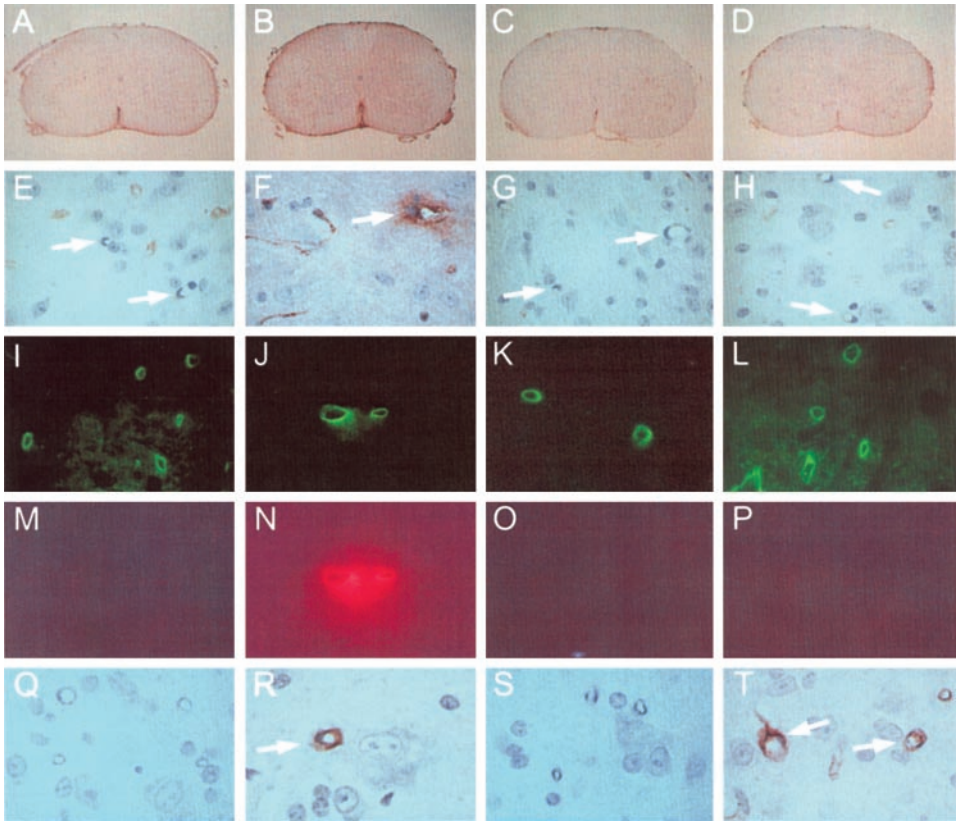

Fig. 4. Assessment of BSCB breakdown in ASMase mice by immunohistochemistry using albumin at 24 h after a 50-Gy dose. In nonirradiated (*A* and *E*) ASMase +/+ mice, no albumin staining was evident (*arrows*). Diffuse albumin staining was seen in the spinal cord of irradiated ASMase +/+ mice (*B*), and albumin immunoreactivity was mainly observed around a microvessel after XRT (*F*; *arrow*). However, no albumin staining was observed in both nonirradiated (*C* and *G*; *arrows*) and irradiated ASMase −/− mice (*D* and *H*; *arrows*). Original magnifications: *A*, *B*, *C*, and *D*, ×25; *E*, *F*, *G*, and *H*, ×1000. BSCB disruption was assessed by use of Evans blue dye. In nonirradiated ASMase +/+ mouse spinal cord (*I*), microvessels, seen in the background (*Ricinus communis* agglutinin-1 immunohistochemistry) showed no leakage of Evans blue dye (*M*). Evans blue dye was observed around microvessels in ASMase +/+ spinal cord at 24 h after 50 Gy (*J* and *N*), but was not observed in nonirradiated (*K* and *O*) or irradiated ASMase −/− animals (*L* and *P*). Original magnifications: ×1000. In nonirradiated p53 +/+ (*Q*) and −/− mice (*S*), no evidence of albumin staining was observed around microvessels. Strong albumin staining was seen around microvessel in the spinal cord of both p53 +/+ (*R*; *arrow*) and −/− mice (*T*; *arrows*) at 24 h after a 50-Gy dose. Original magnifications: ×1000.

at 24 h after XRT in both mouse and rat spinal cord. A 15% loss of endothelial cells in rat brain within 1 day after doses of 25–100 Gy was reported previously by Ljubimova *et al.* (14). In ASMase +/+ mouse spinal cord, the density of endothelial cells showed an almost 50% reduction at 24 h after a 50-Gy dose. The reduction in endothelial cell density observed here in ASMase +/+ mouse spinal cord was greater than that observed in rat brain after XRT. This difference may in part be attributable to methodological differences, *i.e.*, different staining used to identify microvessels and different criteria used for counting endothelial cells. It might also be influenced by differences in species and tissues.

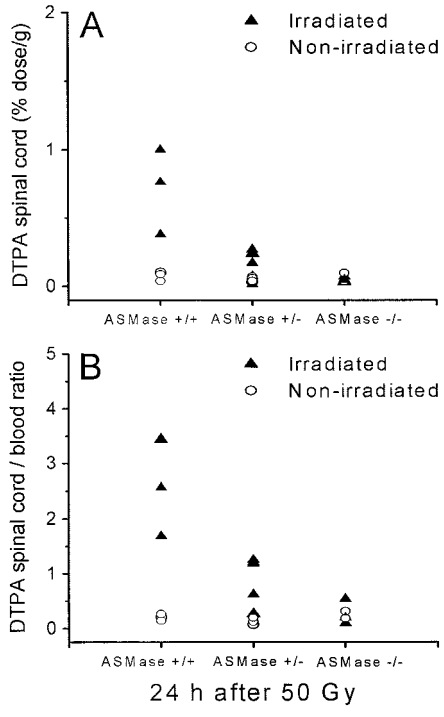

Fig. 5. Quantification of BSCB breakdown in ASMase mice by ^{99m}Tc-DTPA at 24 h after 50 Gy. Results are expressed as the percentage of injected dose/gram of spinal cord (*A*) and as the ratio of ^{99m}Tc-DTPA detected in spinal cord to blood (*B*). Each *data point* represents a measurement from an individual animal.

The early decrease in the number of endothelial cells has been postulated to be attributable to apoptosis of a part of the endothelial population after XRT (2). Our results of a gradual decline in endothelial cell density beginning at 8 or 10 h after XRT were consistent with this notion. In ASMase +/+ mouse spinal cord, there was an almost 50% reduction in endothelial cell density at 24 h after 50 Gy, but no decrease was seen in ASMase −/− mice. Results from this genetic model thus provide definitive proof linking the loss of endothelial cell density to endothelial apoptosis after XRT.

Similar to the results of Peña *et al.* (2), in the present study the apoptotic endothelial cells represented only a small component of the cells undergoing apoptosis after XRT. It is interesting to note that this led to a significant reduction in the endothelial cell population at 24 h after XRT. We have previously shown that the presence of a few apoptotic oligodendrocytes after XRT is also associated with a significant reduction in oligodendroglial density at 24 h after XRT (1). This is consistent with the notion of the very short duration of the apoptotic process *in vivo* (35). For apoptotic endothelial cells, the present methods might also underestimate the actual number of endothelial cells undergoing XRT-induced apoptosis because dying cells shrinking and dislodging away from microvessel walls could be washed away by the blood stream. Moreover, the perfusion procedure used for clearing blood from the circulatory system and tissue fixation in the present study might also wash away some apoptotic endothelial cells and would further limit the detection of apoptotic endothelial cells.

This is the first study demonstrating that endothelial apoptosis is causally associated with acute BSCB disruption after XRT. We observed a dose-dependent reduction in endothelial cell density at 24 h after XRT, which was associated with a similar dose-dependent disruption in BSCB as demonstrated by albumin immunohistochemistry. The dependence of XRT-induced apoptosis of endothelial cells on the ASMase pathway provided us with a genetic approach to address the molecular mechanism of acute BBB disruption induced by XRT. Whereas an almost 50% reduction in endothelial cell density was observed in ASMase +/+ mouse spinal cord at 24 h after a 50-Gy dose, we observed no decrease in ASMase −/− mice. BSCB leakage was evident at 24 h after a 50-Gy dose in ASMase +/+ mouse spinal cord but not in nonirradiated controls and irradiated ASMase −/− mice. These observations provide compelling evidence that XRT-induced endothelial cell apoptosis is causally associated with the acute BSCB disruption after XRT.

We previously demonstrated that oligodendroglial apoptosis after XRT was p53 dependent (36). The reduction in endothelial cell density at 24 h after a 50-Gy dose in p53 +/+ mouse spinal cord was similar to that observed in p53 −/− animals. Consistent with the reduction in endothelial density in both p53 wild-type and knockout animals, p53 +/+ and −/− spinal cord both showed albumin immunoreactivity around microvessels after XRT. We thus conclude that the acute BBB disruption after XRT is mediated by the ASMase but not the p53 pathway. These results suggest that oligodendroglial apoptosis is unlikely to play a critical role in the acute BBB disruption seen after XRT. This is consistent with the notion that astrocytes and microglia, but not oligodendrocytes, contribute to the formation of the BBB (37).

Strategies that elevate cellular ceramide in the sphingomyelinase pathway in initiating XRT-induced apoptosis could be used for clinical radiotherapy aimed to promote apoptosis and improve tumor control. On the other hand, blockage of ceramide generation may protect some normal tissues from the side effects of radiotherapy. When basal fibroblast growth factor was given i.v. immediately before and after XRT, apoptosis was inhibited in endothelial cells in the lungs and mice were protected against the development of lethal XRT pneumonitis (12, 38). More recently, XRT-induced crypt damage, organ failure, and death from the gastrointestinal syndrome were prevented when endothelial apoptosis was inhibited by administration of i.v. basal fibroblast growth factor (13).

For the CNS, our present results indicate that early apoptosis of the microvascular endothelial cell population initiates the development of acute BBB disruption after XRT. Targeting the sphingomyelinase/ceramide pathway may provide a basis for novel neuroprotective strategies. Disruption of the BBB by XRT also has implications in the treatment of primary and secondary brain tumors because it may influence drug delivery to the CNS (39, 40). Targeting XRT-induced endothelial apoptosis and the sphingomyelinase/ceramide pathway may thus be used to increase the permeability of the BBB to improve drug delivery.

ACKNOWLEDGMENTS

We thank Kelvin So and Ye Yang for technical assistance in immunohistochemistry.

REFERENCES

1. Li, Y. Q., Jay, V., and Wong, C. S. Oligodendrocytes in the adult rat spinal cord undergo radiation-induced apoptosis. Cancer Res., *56:* 5417–5422, 1996.
2. Peña, L. A., Fuks, Z., and Kolesnick, R. N. Radiation-induced apoptosis of endothelial cells in the murine central nervous system: protection by fibroblast growth factor and sphingomyelinase deficiency. Cancer Res., *60:* 321–327, 2000.
3. Sheline, G. E., Wara, W. M., and Smith, V. Therapeutic irradiation and brain injury. Int. J. Radiat. Oncol. Biol. Phys., *6:* 1215–1228, 1980.
4. Siegal, T., Pfeffer, M. R., Meltzer, A., Shezen, E., Nimrod, A., Ezov, N., and Ovadia, H. Cellular and secretory mechanisms related to delayed radiation-induced microvessel dysfunction in the spinal cord of rats. Int. J. Radiat. Oncol. Biol. Phys., *36:* 649–659, 1996.
5. Tofilon, P. J., and Fike, J. R. The radioresponse of the central nervous system: a dynamic process. Radiat. Res., *153:* 357–370, 2000.
6. Daigle, J. L., Hong, J. H., Chiang, C. S., and McBride, W. H. The role of tumor necrosis factor signaling pathways in the response of murine brain to irradiation. Cancer Res., *61:* 8859–8865, 2001.
7. Li, Y. Q., Guo, Y. P., Jay, V., Stewart, P. A., and Wong, C. S. Time course of radiation-induced apoptosis in the adult rat spinal cord. Radiother. Oncol., *39:* 35–42, 1996.
8. Bellinzona, M., Gobbel, G. T., Shinohara, C., and Fike, J. R. Apoptosis is induced in the subependyma of young adult rats by ionizing irradiation. Neurosci. Lett., *208:* 163–166, 1996.
9. Shinohara, C., Gobbel, G. T., Lamborn, K. R., Tada, E., and Fike, J. R. Apoptosis in the subependyma of young adult rats after single and fractionated doses of X-rays. Cancer Res., *57:* 2694–2702, 1997.
10. Baker, D. G., and Krochak, R. J. The response of the microvascular system to radiation: a review. Cancer Investig., *7:* 287–294, 1989.
11. Gloor, S. M., Wachtel, M., Bolliger, M. F., Ishihara, H., Landmann, R., and Frei, K. Molecular and cellular permeability control at the blood-brain barrier. Brain Res. Brain Res. Rev., *36:* 258–264, 2001.
12. Fuks, Z., Persaud, R. S., Alfieri, A., McLoughlin, M., Ehleiter, D., Schwartz, J. L., Seddon, A. P., Cordon-Cardo, C., and Haimovitz-Friedman, A. Basic fibroblast growth factor protects endothelial cells against radiation-induced programmed cell death *in vitro* and *in vivo.* Cancer Res., *54:* 2582–2590, 1994.
13. Paris, F., Fuks, Z., Kang, A., Capodieci, P., Juan, G., Ehleiter, D., Haimovitz-Friedman, A., Cordon-Cardo, C., and Kolesnick, R. Endothelial apoptosis as the primary lesion initiating intestinal radiation damage in mice. Science (Wash. DC), *293:* 293–297, 2001.
14. Ljubimova, N. V., Levitman, M. K., Plotnikova, E. D., and Eidus, L. Endothelial cell population dynamics in rat brain after local irradiation. Br. J. Radiol., *64:* 934–940, 1991.
15. Haimovitz-Friedman, A., Kan, C. C., Ehleiter, D., Persaud, R. S., McLoughlin, M., Fuks, Z., and Kolesnick, R. N. Ionizing radiation acts on cellular membranes to generate ceramide and initiate apoptosis. J. Exp. Med., *180:* 525–535, 1994.
16. Haimovitz-Friedman, A., Balaban, N., McLoughlin, M., Ehleiter, D., Michaeli, J., Vlodavsky, I., and Fuks, Z. Protein kinase C mediates basic fibroblast growth factor protection of endothelial cells against radiation-induced apoptosis. Cancer Res., *54:* 2591–2597, 1994.
17. Lozano, J., Menendez, S., Morales, A., Ehleiter, D., Liao, W. C., Wagman, R., Haimovitz-Friedman, A., Fuks, Z., and Kolesnick, R. Cell autonomous apoptosis defects in acid sphingomyelinase knockout fibroblasts. J. Biol. Chem., *276:* 442–448, 2001.
18. Kolesnick, R., and Fuks, Z. Ceramide: a signal for apoptosis or mitogenesis? J. Exp. Med., *181:* 1949–1952, 1995.
19. Levade, T., and Jaffrezou, J. P. Signalling sphingomyelinases: which, where, how and why? Biochim. Biophys. Acta, *1438:* 1–17, 1999.
20. Jaffrezou, J. P., Bruno, A. P., Moisand, A., Levade, T., and Laurent, G. Activation of a nuclear sphingomyelinase in radiation-induced apoptosis. FASEB J., *15:* 123–133, 2001.
21. Zundel, W., Swiersz, L. M., and Giaccia, A. Caveolin 1-mediated regulation of receptor tyrosine kinase-associated phosphatidylinositol 3-kinase activity by ceramide. Mol. Cell. Biol., *20:* 1507–1514, 2000.
22. Peña, L. A., Fuks, Z., and Kolesnick, R. Stress-induced apoptosis and the sphingomyelin pathway. Biochem. Pharmacol., *53:* 615–621, 1997.
23. Santana, P., Peña, L. A., Haimovitz-Friedman, A., Martin, S., Green, D., McLoughlin, M., Cordon-Cardo, C., Schuchman, E. H., Fuks, Z., and Kolesnick, R. Acid sphingomyelinase-deficient human lymphoblasts and mice are defective in radiation-induced apoptosis. Cell, *86:* 189–199, 1996.
24. Horinouchi, K., Erlich, S., Perl, D. P., Ferlinz, K., Bisgaier, C. L., Sandhoff, K., Desnick, R. J., Stewart, C. L., and Schuchman, E. H. Acid sphingomyelinase deficient mice: a model of types A and B Niemann-Pick disease. Nat. Genet., *10:* 288–293, 1995.
25. Wong, C. S., Minkin, S., and Hill, R. P. Linear-quadratic model underestimates sparing effect of small doses per fraction in rat spinal cord. Radiother. Oncol., *23:* 176–184, 1992.
26. Goffinet, D. R., Marsa, G. W., and Brown, J. M. The effects of single and multifraction radiation courses on the mouse spinal cord. Radiology, *119:* 709–713, 1976.
27. Goffinet, D. R., Choi, K. Y., and Brown, J. M. The combined effects of hyperthermia and ionizing radiation on the adult mouse spinal cord. Radiat. Res., *72:* 238–245, 1977.
28. Habermalz, H. J., Valley, B., and Habermalz, E. Radiation myelopathy of the mouse spinal cord: isoeffect correlations after fractionated radiation. Strahlenther. Onkol., *163:* 626–632, 1987.
29. Li, Y. Q., and Wong, C. S. Radiation-induced apoptosis in the neonatal and adult rat spinal cord. Radiat. Res., *154:* 268–276, 2000.
30. Li, Y. Q., Ballinger, J. R., Nordal, R. A., Su, Z. F., and Wong, C. S. Hypoxia in radiation-induced blood-spinal cord barrier breakdown. Cancer Res., *61:* 3348–3354, 2001.

31. Ng, S. S., Tsao, M. S., Nicklee, T., and Hedley, D. W. Wortmannin inhibits pkb/akt phosphorylation and promotes gemcitabine antitumor activity in orthotopic human pancreatic cancer xenografts in immunodeficient mice. Clin. Cancer Res., *7:* 3269–3275, 2001.
32. Fullerton, S. M., Shirman, G. A., Strittmatter, W. J., and Matthew, W. D. Impairment of the blood-nerve and blood-brain barriers in apolipoprotein e knockout mice. Exp. Neurol., *169:* 13–22, 2001.
33. Stewart, P. A., Vinters, H. V., and Wong, C. S. Blood-spinal cord barrier function and morphometry after single doses of x-rays in rat spinal cord. Int. J. Radiat. Oncol. Biol. Phys., *32:* 703–711, 1995.
34. Bar, T. Morphometric evaluation of capillaries in different laminae of rat cerebral cortex by automatic image analysis: changes during development and aging. Adv. Neurol., *20:* 1–9, 1978.
35. Barres, B. A., Hart, I. K., Coles, H. S., Burne, J. F., Voyvodic, J. T., Richardson, W. D., and Raff, M. C. Cell death and control of cell survival in the oligodendrocyte lineage. Cell, *70:* 31–46, 1992.
36. Chow, B. M., Li, Y. Q., and Wong, C. S. Radiation-induced apoptosis in the adult central nervous system is p53-dependent. Cell Death Differ., *7:* 712–720, 2000.
37. Prat, A., Biernacki, K., Wosik, K., and Antel, J. P. Glial cell influence on the human blood-brain barrier. Glia, *36:* 145–155, 2001.
38. Fuks, Z., Alfieri, A., Haimovitz-Friedman, A., Seddon, A., and Cordon-Cardo, C. Intravenous basic fibroblast growth factor protects the lung but not mediastinal organs against radiation-induced apoptosis *in vivo.* Cancer J. Sci. Am., *1:* 62–72, 1995.
39. Qin, D., Ou, G., Mo, H., Song, Y., Kang, G., Hu, Y., and Gu, X. Improved efficacy of chemotherapy for glioblastoma by radiation-induced opening of blood-brain barrier: clinical results. Int. J. Radiat. Oncol. Biol. Phys., *51:* 959–962, 2001.
40. van Vulpen, M., Kal, H. B., Taphoorn, M. J., and El-Sharouni, S. Y. Changes in blood-brain barrier permeability induced by radiotherapy: implications for timing of chemotherapy? Oncol. Rep., *9:* 683–688, 2002.